catalysts

MDPI

Article

Efficient Photodegradation of Congo Red and Phenol Red in Wastewater Using Nanosized Cu-Polyoxometalate: A Promising UV-Active Catalyst for Environmental Treatment

Suhair A. Bani-Atta [1], Ahmed Ali A. Darwish [2,*], Nada M. Alatawi [3], Nada D. Alkhathami [3], Jozaa N. Al-Tweher [3] and Eman F. M. El-Zaidia [2]

[1] Analytical Chemistry Research Laboratory, Department of Chemistry, Faculty of Science, University of Tabuk, Tabuk 71491, Saudi Arabia; s_bantatta@ut.edu.sa
[2] Advanced Materials Research Laboratory, Department of Physics, Faculty of Science, University of Tabuk, Tabuk 71491, Saudi Arabia; e_ali@ut.edu.sa
[3] Department of Chemistry, Faculty of Science, University of Tabuk, Tabuk 71491, Saudi Arabia
* Correspondence: aadarwish@ut.edu.sa

Abstract

This research focuses on the synthesis, characterization, and photocatalytic performance of Cu-based polyoxometalate (Cu-POM) as an effective catalyst for the degradation of organic dyes, specifically Congo Red (CR) and Phenol Red (PR). The main goals are to synthesize Cu-POM using a controlled self-assembly technique, characterize its optical and structural characteristics using FTIR, XRD, SEM, TGA, and UV-Vis spectroscopy, and estimate its photocatalytic activity when exposed to UV light. The outcomes confirm the successful formation of Cu-POM with well-defined nanostructures and a crystalline polyoxometalate framework. The determined optical bandgap of 3.65 eV indicates its strong UV-light responsiveness. The photocatalytic degradation experiments demonstrated high removal efficiencies of 58.1% for CR and 64.6% for PR under UV irradiation, corresponding kinetic rate constants of 0.00484 min^{-1} and 0.00579 min^{-1}, respectively. The superior photocatalytic activity is attributed to the efficient charge carrier separation and high surface area of Cu-POM. These findings highlight the potential of Cu-POM as a promising heterogeneous photocatalyst for sustainable wastewater treatment and environmental remediation.

Keywords: polyoxometalate; photocatalysis; degradation; congo red; phenol red

check for updates

Academic Editors: Mónica L. Casella, Ileana Daniela Lick and Paula Osorio-Vargas

Received: 4 August 2025
Revised: 16 September 2025
Accepted: 22 September 2025
Published: 25 September 2025

Citation: Bani-Atta, S.A.; Darwish, A.A.A.; Alatawi, N.M.; Alkhathami, N.D.; Al-Tweher, J.N.; El-Zaidia, E.F.M. Efficient Photodegradation of Congo Red and Phenol Red in Wastewater Using Nanosized Cu-Polyoxometalate: A Promising UV-Active Catalyst for Environmental Treatment. *Catalysts* **2025**, *15*, 920. https://doi.org/10.3390/catal15100920

Copyright: © 2025 by the authors. Licensee MDPI, Basel, Switzerland. This article is an open access article distributed under the terms and conditions of the Creative Commons Attribution (CC BY) license (https://creativecommons.org/licenses/by/4.0/).

1. Introduction

In recent years, the escalating concerns regarding the discharge of approximately 280,000 tons of textile dyes into industrial wastewater annually by the textile industry have raised significant environmental issues [1]. During the dyeing process, about 15–20% of the total synthetic dye production is lost, including dyes such as Methylene blue (MB), Congo red (CR), Phenol Red (PR), Methyl orange (MO), Methylene red (MR), Rhodamine B (RhB), Remazol brilliant blue (RB), and numerous other dyes [2,3]. These dyes are often discharged into the aquatic systems without further treatment, causing significant environmental harm [4]. Due to their complex chemical structures, most synthetic dyes are toxic and highly resistant to degradation. These dyes are widely used in leather, textile dyeing, color photography, food, pharmaceutical, and cosmetic industries [5–7].

Generally, synthetic dyes display a stable structure and a remarkable affinity for water and organic solvents [8,9]. Even at small concentrations, their presence in aquatic systems poses a significant risk to ecosystems and can have mutagenic effects on human

health [10]. Various chemical and physical methods have been effectively employed to decontaminate wastewater from dyes [11,12]. Among these, adsorption technology is widely applied [13–16], with activated carbon being one of the most elucidated, effective, and commonly employed adsorbents. However, challenges remain, including the prohibitive cost of economics, the preparation of adsorbents, and the steps required for their removal after treatment. There is a pressing need to develop and implement innovative methods for treating wastewater contaminated with dyes and other pollutants [17,18].

The molecular structure of synthetic dyes significantly influences their chemical stability, solubility, and degradation behavior. As illustrated in Figure 1, dyes such as CR and PR contain complex conjugated systems with aromatic rings and functional groups, enhancing their stability and degradation resistance. CR, a diazo dye, consists of two azo (-N=N) linkages bridging aromatic moieties, facilitating electron delocalization, and increasing photostability. PR, a sulfone phthalein dye, features a rigid molecular framework with extensive π-conjugation, contributing to its distinct color variation in response to pH changes. These structural characteristics influence their interaction with solvents and determine their degradation pathways under photocatalytic conditions. Understanding these molecular features is essential for optimizing photocatalytic strategies and selecting suitable catalysts for effective dye removal.

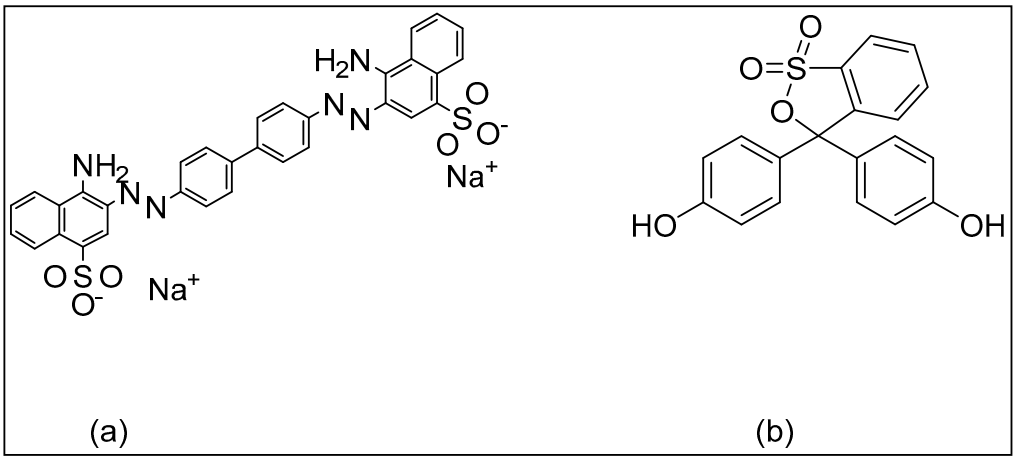


Figure 1. (**a**) The structure of the Congo Red (CR) and (**b**) Phenol Red (PR).

Conventional wastewater treatment techniques, including adsorption, coagulation, and chemical oxidation, often suffer from high costs, incomplete degradation, or secondary pollution. Given the limitations of conventional dye removal methods, researchers have turned to advanced oxidation processes, particularly photocatalysis, as a promising and environmentally friendly alternative for wastewater treatment [19,20]. Traditional photocatalysts such as TiO_2 and ZnO have been extensively studied for dye degradation. However, they suffer from significant drawbacks, including high charge recombination rates, limited absorption in the visible spectrum, and insufficient long-term stability. Additionally, ZnO is prone to photo-corrosion, reducing its efficiency over time. These challenges necessitate exploring alternative materials with improved stability, charge separation efficiency, and light absorption capabilities.

Polyoxometalates (POMs) have gained significant attention due to their unique, exceptional properties, including high stability, tunable structural versatility, and remarkable photocatalytic activity [21,22]. Characterized by their unique molecular structures comprising metal-oxygen clusters [23], POMs exhibit remarkable photocatalytic properties under light irradiation. This has motivated extensive research into their potential as catalysts for the degradation of organic dyes in aqueous systems [24]. By photocatalysis, the interac-

tion between POMs and organic dyes generates reactive oxygen species (ROS) and other oxidative species, which initiate the degradation process [25,26]. This approach offers an environmentally friendly method for dye removal and contributes to the overall remediation of water bodies contaminated by industrial effluents. Despite these advantages, many POMs exhibit limited reusability and require further modification to enhance their photocatalytic activity.

Copper-substituted POMs (Cu-POMs) are a well-established method for improving catalytic performance [27]. Cu ions can be incorporated into the POM framework at lacunary or substituted sites, helping with charge separation and increasing the production of reactive oxygen species (ROS) under light exposure [28]. However, research on Cu-POMs remains limited, especially regarding their structural stability, photocatalytic processes, and practical uses in wastewater treatment.

This study focuses on synthesizing and characterizing nanosized Cu-POM and its application in the photodegradation of CR and PR dyes under UV irradiation. With its well-defined nanostructure, high surface area, and tunable electronic properties, we hypothesize that Cu-POM will exhibit superior photocatalytic efficiency compared to conventional catalysts. By systematically evaluating its degradation kinetics, optical properties, and stability, this study advances the understanding of POM-based photocatalysts and demonstrates their potential for large-scale wastewater treatment applications.

2. Results and Discussions

2.1. Characterization of Cu-POM Cluster

Figure 2 displays the FTIR bands of Cu-POM, illustrating the surface functional groups of the metal polyoxometalate. The broad absorption band observed around 3425.13 cm^{-1} corresponds to the O-H stretching vibration of water molecules adsorbed on the surface polyoxometalate framework. The band at 1619.99 cm^{-1} is attributed to the bending vibration of H_2O molecules, indicating the presence of hydration water. The characteristic peaks of polyoxometalates (POMs) appear in the lower wavenumber region. Specifically, the absorption band at 933.42 cm^{-1} can be assigned to the asymmetric stretching vibrations of W=O bonds.

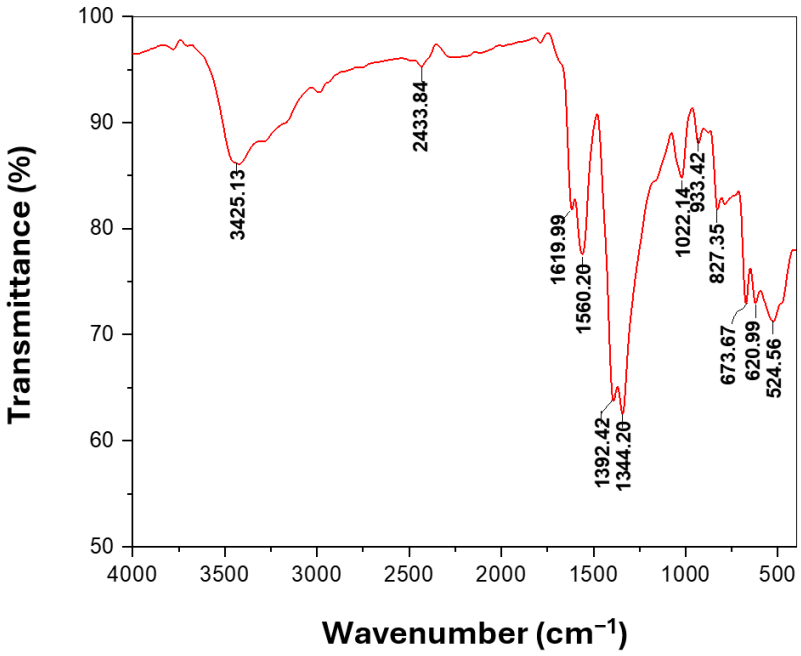


Figure 2. FTIR spectrum of Cu-POM.

In contrast, the band at 827.35 cm^{-1} corresponds to W-O-W bridging vibrations, confirming the Keggin-type structure of Cu-POM [29]. The presence of additional peaks in the range of 500–800 cm^{-1} indicates the coordination of Cu^{2+} within the polyanion, likely through Cu-O-W interactions. These findings align with previous studies on metal-incorporated polyoxometalates, demonstrating their potential as effective photocatalysts [29,30]. These findings are consistent with earlier studies on POM-based catalysts, where such distinctive bands confirm the integrity and stability of polyoxometalate frameworks [31]. The successful synthesis and characterization of Cu-POM through FTIR analysis highlights its potential application in photocatalysis and environmental remediation [30].

The thermal stability of the Cu-POM compound was investigated using thermogravimetric analysis (TGA) over a temperature range of 30–800 °C, as shown in Figure 3. The TGA curve reveals three distinct weight loss stages. The first stage (50–150 °C) corresponds to the removal of physically adsorbed water [32], with a weight loss of ≈10%. The second stage (150–300 °C) is attributed to the elimination of chemically bound water and hydroxyl groups [33], contributing to a further ≈20% weight loss. The third stage (300–600 °C) corresponds to the decomposition of the organic framework [32], resulting in an additional ≈5% weight loss. Beyond 600 °C, the residual weight remains nearly constant, indicating the high thermal stability and robustness of the Cu-POM inorganic framework.

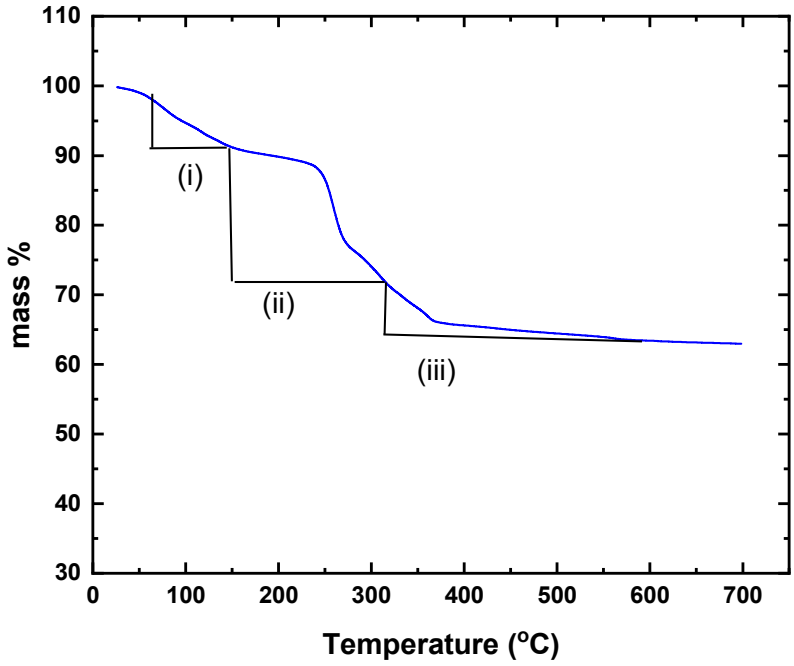


Figure 3. Thermogravimetric analysis (TGA) of Cu-POM.

X-ray diffraction (XRD) is an essential technique for analyzing the purity of crystalline materials, phase composition, and structural properties. The successful synthesis of Cu-POM is confirmed by XRD analysis conducted in the current study. The crystalline structure of the synthesized Cu-POM was examined using XRD, and the results are shown in Figure 4. The pattern exhibits sharp diffraction peaks at 35.3° and 38.8°, corresponding to the (11-1), (111), and (220) planes of Cu/CuO, in agreement with the JCPDS card No. 48-1548 [34]. While strong Cu/CuO reflections are observed, the weaker broad reflections near 27.2° and 50–57° are characteristic of Keggin-type POM units. Similar patterns have been reported in other transition-metal-substituted POMs, where strong scattering from incorporated metal species overshadows the weaker POM framework reflections. This confirms that the synthesized material is a hybrid Cu-POM composite rather than a simple physical mixture.

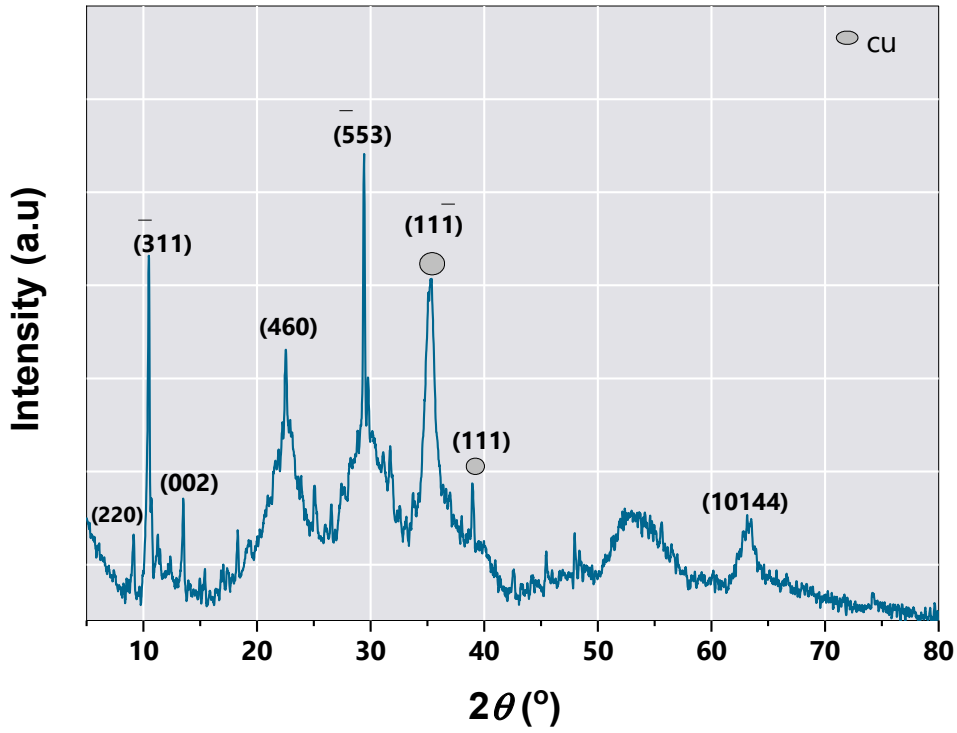
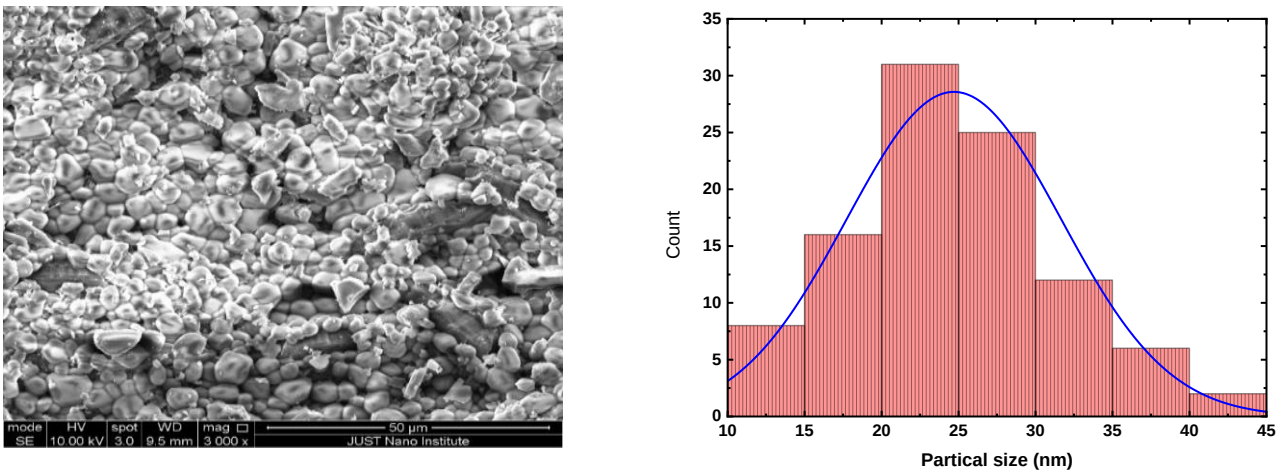


Figure 4. XRD patterns of Cu-POM.

In contrast, the characteristic reflections of the polyoxometalate (POM) framework are observed as weaker and broader features in the 2θ region of 25–30°, consistent with the semi-crystalline nature of Keggin-type POM units [35]. The broad reflection near 27.2° can be considered the structural fingerprint of the POM cluster, which has been reported for other transition-metal-substituted POMs [35]. In addition, a broad diffraction feature is observed in the range of 50–57°, which does not correspond to Cu or CuO phases. This band is attributed to diffuse scattering from the semi-crystalline POM framework and possible overlapping weak reflections of W–O and Bi–O coordination environments [21]. Such features have been previously reported for POM-based composites, where the strong scattering contribution of incorporated metal ions often overshadows the weaker reflections of the POM framework [23]. Overall, the coexistence of sharp Cu/CuO peaks and weaker POM reflections demonstrates that the synthesized Cu-POM successfully integrates metallic copper with a polyoxometalate framework. This hybrid crystallinity ensures both structural stability and enhanced catalytic activity, consistent with reported POM-based photocatalysts.

High crystallinity is demonstrated by well-defined and sharp diffraction, which is very important for the preservation of the functional qualities of Cu-POM in electrochemical and catalytic applications. The SEM image of Cu-POM (Figure 5a) reveals a noticeable accumulation of small, highly uniform nanoparticles, suggesting a degree of agglomeration. The individual particles are primarily spherical, although some exhibit angular features or minor faceting. This is typical for crystalline POM structures. The surface texture appears relatively smooth, and this is essential for ensuring effective catalytic interactions. Some particles appear to be agglomerated to some extent, which is common in nanomaterials. However, overall morphology suggests a controlled synthesis process, resulting in particles with high degrees of structural integrity. The distribution curve of the particle size distribution of Cu-POM (Figure 5b) indicates that the average particle size of Cu-POM is approximately 24 nm. This narrow distribution is significant because it suggests a high level of homogeneity. Smaller particle sizes generally provide a larger surface area, enhancing

the material's reactivity and efficiency in processes such as dye degradation, water splitting, or organic synthesis due to increased active sites and improved light absorption [36,37].



(**a**) (**b**)

Figure 5. (**a**) SEM image and (**b**) particle size distribution of Cu-POM.

The particle size distribution obtained from SEM analysis indicates an average diameter of ≈24 nm with relatively narrow dispersion. Although TEM and EDX mapping would provide further validation of morphology and elemental homogeneity, such measurements could not be performed in the present study due to instrumental limitations. Nevertheless, the combination of SEM, XRD, FTIR, and TGA analyses provides consistent evidence for the successful formation of nanosized Cu-POM. These techniques have also been widely employed in previous studies of POM-based nanostructures [23].

The optical properties of the Cu-POM compound were analyzed using UV-Vis spectroscopy, as shown in Figure 6a. The absorbance spectrum exhibits a strong absorption band in the UV region, indicating that the electronic transitions of metal-oxygen bonds occur within the Cu-POM structure. This absorption behavior is characteristic of polyoxometalate materials, particularly ligand-to-metal charge transfer (LMCT) [38]. This behavior aligns with previous studies on transition metal-incorporated POMs, which exhibit strong absorption due to metal-to-ligand charge transfer (MLCT) transitions [39]. The optical band gap energy (E_g) of Cu-POM was determined using Tauc's plot (Figure 6b) by plotting $(\alpha E)^{(1/2)}$ versus photon energy (E), where α is the absorption coefficient, and n depends on the type of electronic transition. The estimated bandgap of Cu-POM (3.65 eV) is slightly higher than the value of 3.29 eV reported for similar POM-based systems [24]. This variation can be attributed to differences in particle size, degree of metal incorporation, and synthesis parameters, which influence electronic structure and light absorption. Notably, the average particle size of Cu-POM in this study (~24 nm, Figure 5b) may induce mild quantum confinement effects, resulting in a bandgap widening compared to bulk counterparts. Similar observations of bandgap shift due to the nanoscale impacts have been reported in polyoxometalates and related photocatalysts [23,38].

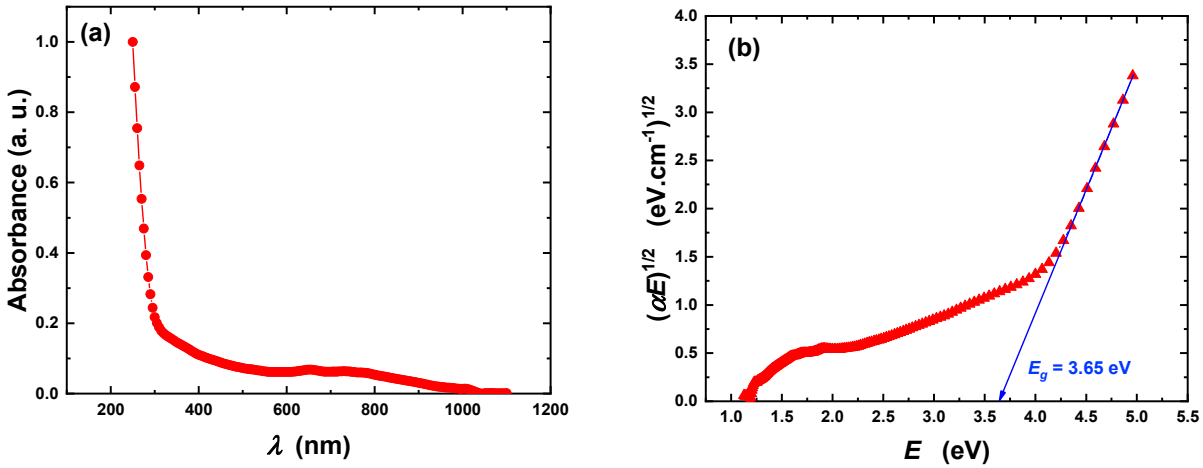


Figure 6. (**a**) Absorbance spectrum of Cu-POM solution and (**b**) Tauc's relation to determining energy bandgap.

2.2. Photocatalysis Investigations of Cu-POM

The photocatalytic performance of Cu-POM was examined through the degradation of CR and PR dyes under UV irradiation. Figure 7 shows the absorbance spectra of CR and PR dyes at different UV irradiation times in the presence of the Cu-POM catalyst. The CR and PR solutions initially exhibit distinct absorption peaks at 497 and 443 nm, respectively, corresponding to their characteristic absorption peaks. However, as the irradiation time increases, these peaks diminish, showing the breakdown of dye molecules due to the catalytic activity of Cu-POM. This decrease in absorbance suggests that Cu-POM facilitates the degradation process by generating reactive species under UV light, which attack and decompose the dye structures. These findings align with previous studies on polyoxometalate-based catalysts [31,40]. The variation in degradation rates between CR and PR may be attributed to molecular structure differences, catalyst interaction, and photostability. These findings highlight the potential of Cu-POM as an efficient photocatalyst for dye removal from wastewater.

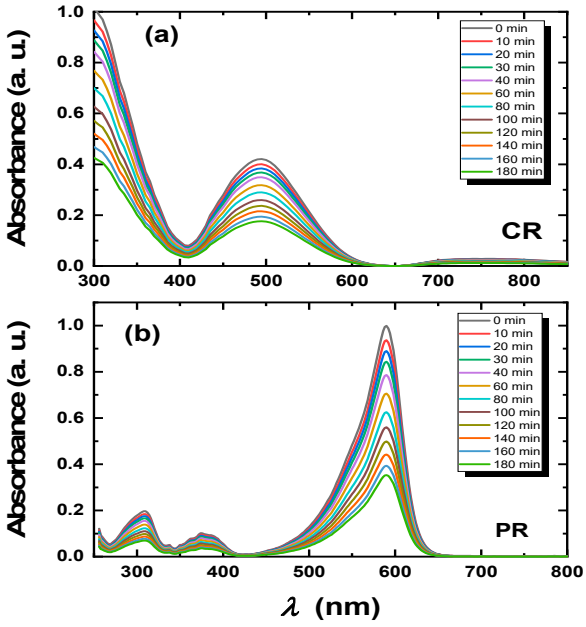


Figure 7. Absorbance of (**a**) CR and (**b**) PR dyes at different UV irradiation times with Cu-POM catalyst.

The decrease in absorbance is attributed to the generation of electron-hole pairs (e^--h^+) in Cu-POM under UV irradiation. These charge carriers react with water and oxygen molecules to produce reactive oxygen species (ROS), such as •OH and $•O_2^-$, which attack and break down the dye molecules [27,41,42]. Cu-POM has a suitable bandgap energy that allows it to absorb UV light efficiently, making it an effective photocatalyst for dye degradation. Additionally, the high surface area and uniform particle size distribution of Cu-POM (as shown in Figure 5) enhance its photocatalytic performance by providing more active sites for dye adsorption and degradation [36].

Figure 8 shows the concentration decay curves of CR and PR dyes as a function of UV irradiation time in the presence of the Cu-POM catalyst. The curves show a rapid decrease in the concentration of both dyes with increasing UV irradiation time, highlighting the efficiency of Cu-POM in catalyzing the degradation of organic dyes. Notably, the concentration of PR decreases more rapidly than that of CR over the same period, indicating a higher photocatalytic degradation efficiency for PR. This disparity in degradation rates can be attributed to differences in the molecular structures of the dyes, which influence their interactions with the catalyst and their susceptibility to oxidative processes. A sharp decline in the concentration of CR and PR dyes is observed even during the initial minutes of UV irradiation. For example, after 60 min, the concentration drops to approximately 80% of its initial value. After a longer irradiation time of 130 min, the rate of concentration decrease slows down, indicating that the reaction is approaching equilibrium, where most of the dye has been degraded, and minor compounds have been formed.

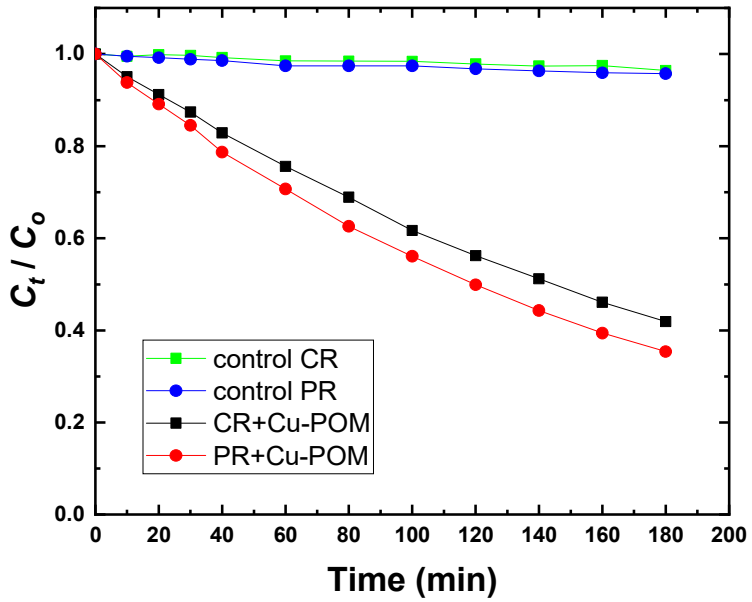


Figure 8. Concentration decay of CR and PR dyes by Cu-POM catalyst at different UV irradiation times.

This is one of the pioneering studies demonstrating the ability of the POMs to photodegrade PR dye. This promising result may open the door for future research in the decomposition of neutral dyes, such as PR dye, using Cu-POM as a photocatalyst. Similar studies have demonstrated the efficacy of copper-based catalysts in the photodegradation of CR dye. For instance, Abdulnabi et al. reported that g-C_3N_4@PMA/AgCl particles effectively degrade CR under visible light irradiation [43]. Moreover, Rasheed et al. (2021) found that Cu_2O and CuO nanoparticles exhibit significant photocatalytic activity toward CR degradation [44]. The degradation kinetics in Figure 8 suggest that the Cu-POM catalyst facilitates the generation of reactive species under UV light, leading to the breakdown

of dye molecules. This aligns with findings by Abdulnabi et al. (2023), who observed that their POMs materials possess enhanced visible light absorption and efficient charge separation properties, contributing to their photocatalytic performance [43].

Figure 9 illustrates the photocatalytic efficiency of the Cu-POM catalyst over time. The data indicate a higher degradation efficiency for PR than CR, suggesting that PR is more susceptible to photocatalytic breakdown under the given conditions. This observation aligns with previous studies that have reported varying degradation efficiencies for different dyes when subjected to photocatalysis [43,44].

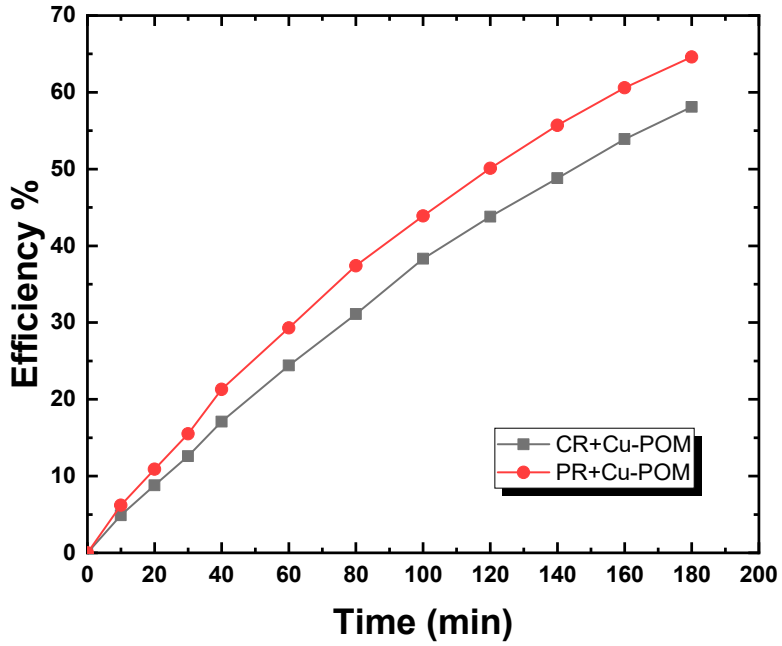


Figure 9. The photocatalytic efficiency of CR and PR dyes by Cu-POM catalyst at different UV irradiation.

The degradation kinetics of CR and PR dyes were analyzed using the pseudo–first-order model, which is commonly applied in photocatalytic systems. The model is expressed as [24]:

$$n\left(\frac{C_t}{C_o}\right) = -k_{app}\, t \quad (1)$$

where C_o and C_t represent the dye concentrations at initial time and at time t, respectively, and k_{app} is the apparent rate constant (min^{-1}).

The relationship between $\ln(C_t/C_o)$ and time for both CR and PR dyes was studied and presented in Figure 10, providing a kinetic analysis of the degradation process. The linearity of these plots suggests that the degradation follows pseudo-first-order kinetics, a common characteristic in photocatalytic dye degradation studies. The steeper slope observed for PR indicates a faster degradation rate than CR. This kinetic behavior is consistent with findings from other research, such as the work by Arora et al., which reported enhanced degradation rates for certain dyes due to the specific interactions between the dye molecules and the photocatalyst surface [45]. The differences in degradation rates between CR and PR can be attributed to their distinct molecular structures, which affect their adsorption onto the catalyst surface and their reactivity under UV light. Understanding these variations is crucial for optimizing photocatalytic processes for wastewater treatment applications.

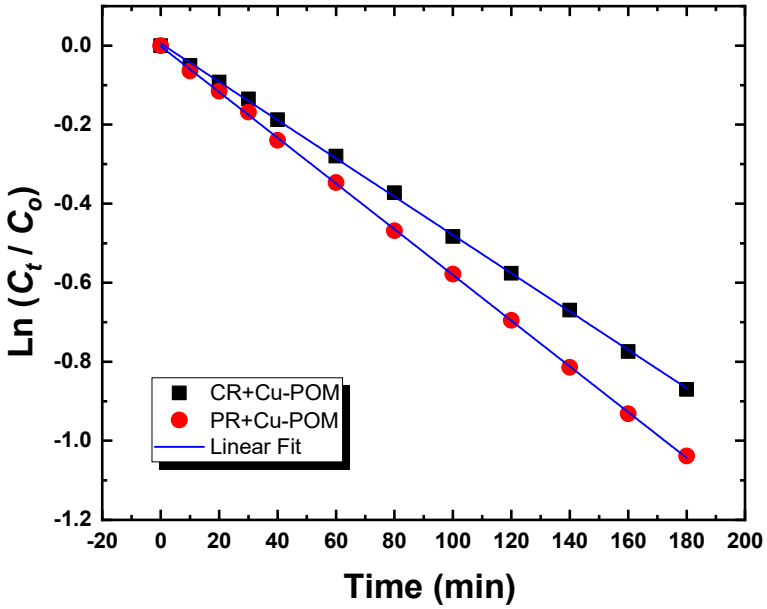
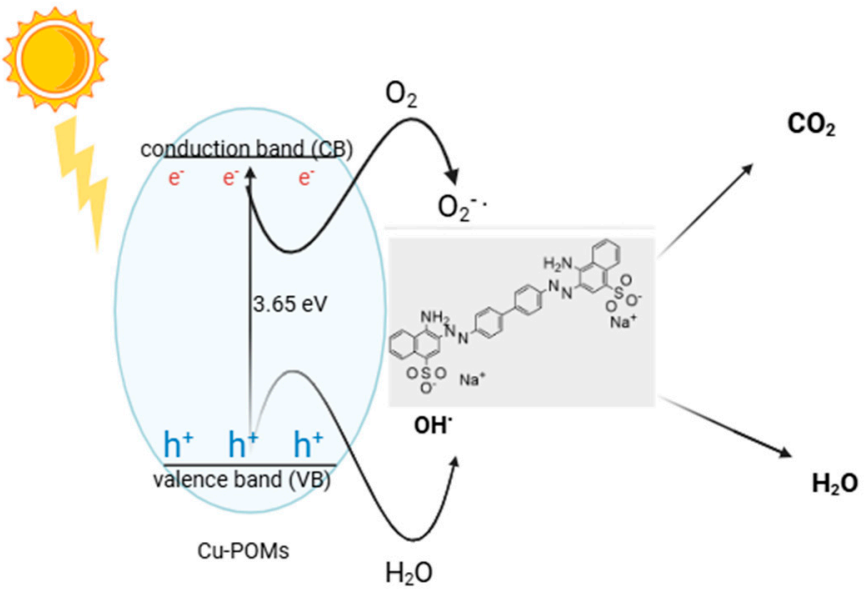


Figure 10. The relation between ln(C_t/C_o) and time for CR and PR dyes by Cu-POM catalyst at different UV.

3. Mechanism of Photocatalytic Degradation

Polyoxometalates (POMs) possess a semiconductor-like electronic structure characterized by an electron-filled valence band (VB) and an empty conduction band (CB). The estimated band gap for the used photocatalysts is 3.65 eV, suitable for degrading organic dyes like CR and PR. The photocatalytic mechanism of POM catalysts is like that of TiO_2 and other photocatalytic materials [41]. When the catalyst is irradiated with energy equal to or greater than its bandgap, electrons are excited from the VB to the CB, generating electrons (e^-) and holes (h^+), Scheme 1. The photogenerated electrons (e^-) are captured by oxygen molecules, resulting in $O_2^-\bullet$ species. Positive holes produce hydroxyl radicals (·OH) when they react with water and organic CR and PR dyes. These species initiate photocatalytic reactions, attracting PR and CR molecules and breaking them into simpler compounds [46,47].



Scheme 1. The suggested photocatalytic pathways include the concurrent oxidation of CR dye facilitated by the Cu–POM catalyst.

Polyoxometalates (POMs) possess a semiconductor-like electronic structure characterized by an electron-filled valence band (VB) and an empty conduction band (CB) [48].

When Cu-POM is irradiated with UV light of sufficient energy (≥3.65 eV), it undergoes photoexcitation, generating electron-hole pairs:

$$\mathrm{Cu-POM} + h\nu \rightarrow \mathrm{Cu-POM}\left(\mathrm{e^-}_{\mathrm{CB}} + \ h^+_{\mathrm{VB}}\ \right)$$

The photogenerated electrons (e^-) in the conduction band (CB) can react with oxygen molecules adsorbed on the catalyst surface, forming superoxide radicals ($\cdot O_2{}^-$):

$$\mathrm{e^-}_{\mathrm{CB}} + \mathrm{O_2} \ \rightarrow \ \cdot \mathrm{O_2}^-$$

These superoxide radicals can undergo further reactions, forming hydrogen peroxide (H_2O_2), which decomposes into hydroxyl radicals ($\cdot OH$):

$$\cdot \mathrm{O_2}^- + \mathrm{H_2O} \rightarrow \mathrm{HO_2} + \mathrm{OH^-}$$
$$2\mathrm{HO_2} \rightarrow \mathrm{H_2O_2} + \mathrm{O_2}$$
$$\mathrm{H_2O_2} \rightarrow 2\ \mathrm{OH^-}$$

Simultaneously, the holes (h^+) in the valence band (VB) have strong oxidative potential and directly react with water molecules to produce hydroxyl radicals:

$$\mathrm{h^+}_{\mathrm{VB}} \ + \mathrm{H_2O} \rightarrow \cdot \mathrm{OH} + \mathrm{H^+}$$

Hydroxyl radicals ($\cdot OH$) and superoxide radicals ($\cdot O_2{}^-$) are highly reactive species that attack and degrade dye molecules (CR and PR) into smaller, non-toxic products:

$$\cdot \mathrm{OH} + \mathrm{CR/PR} \rightarrow \text{Degraded products}$$

Incorporating Cu^{2+} ions in Cu-POM facilitates better electron mobility, reducing charge recombination and increasing the lifetime of photoexcited electrons [49]. This enhances the generation of reactive oxygen species (ROS). Cu^{2+} ions can serve as an electron mediator, accepting and transferring photogenerated electrons to absorbed oxygen, improving the formation of superoxide radicals:

$$\mathrm{Cu^{2+}} + \mathrm{e^-}_{\mathrm{CB}} \rightarrow \mathrm{Cu^+}$$
$$\mathrm{Cu^+} + \mathrm{O_2} \rightarrow \mathrm{Cu^{2+}} + \cdot \mathrm{O_2^-}$$

The presence of Cu in the polyoxometalate framework increases the number of active sites for dye adsorption and reaction, improving overall photocatalytic efficiency.

4. Comparison with Previous Studies

The photocatalytic degradation of organic dyes has been extensively investigated using various semiconductor materials, metal oxides, and POM-based catalysts. The present study highlights the efficiency of the synthesized Cu-POM nanocomposite in degrading CR and PR under UV irradiation. Table 1 compares previously reported photocatalysts for CR and PR removal to contextualize the performance of Cu-POM.

Table 1. Comparison of values for photocatalytic efficiency and rate kinetic constant with values for dye removal reported in the literature [a].

Catalytic	Dye	PCE%	k_{app} (min^{-1})	Reference
Cu-POM	CR	58.1	0.00484	Current work
Cu-POM	PR	64.6	0.00579	Current work
Mg/Al-TiO_2	CR	73		[47]
ZnAl-[$SiW_{12}O_{40}$]	CR	66		[31]
ZnAl-[$PW_{12}O_{40}$]	CR	73		[31]
MgAl-[$PW_{12}O_{40}$]	CR	73		[31]
WO_3 nanocrystal	CR	60		[50]
CoV POMs/PMS	PR	70.3		[40]

[a]: Reported values are under their respective experimental conditions.

The results demonstrate that Cu-POM exhibits a photocatalytic efficiency (PCE) of 58.1% for CR and 64.6% for PR, along with corresponding apparent rate constants (k_{app}) of 0.00484 min^{-1} and 0.00579 min^{-1}. These values indicate a competitive degradation efficiency, positioning Cu-POM among the promising photocatalysts for dye removal. Compared to other reported catalysts, Mg/Al-TiO_2 and ZnAl-[$PW_{12}O_{40}$] exhibited relatively high removal efficiencies (~73% for CR), while WO_3 nanocrystals achieved around 60% degradation after 180 min. CoV-POMs/PMS, another polyoxometalate-based system, notably demonstrated a slightly higher PR degradation efficiency (70.3%). Yet, the Cu-POM catalyst in the present work offers a significant advantage in terms of synthesis simplicity and UV activation.

Additionally, ZnAl- and MgAl-based polyoxometalate composites have been reported to exhibit notable degradation efficiencies, yet their k_{app} values are often not explicitly stated in the literature. This makes direct kinetic comparisons challenging. However, considering the structural modifications introduced in Cu-POM, particularly the integration of Cu ions within the POM framework, the enhanced electron transfer dynamics and photogenerated charge separation likely contribute to its superior photocatalytic performance. Overall, the findings of this study affirm that Cu-POM presents a highly efficient and stable photocatalyst for removing PR and CR dyes. The combination of POM stability, Cu-induced charge transfer enhancement, and strong UV absorption underscores the potential of Cu-POM in advanced wastewater treatment technologies. Further research could explore extending its activity to visible-light-driven photodegradation, thereby broadening its practical applications in environmental remediation.

Compared with other reported POM-based photocatalysts, the present Cu-POM system exhibits several advantages. First, the incorporation of Cu^{2+} ions into the POM framework enhances electron mobility and reduces charge recombination, leading to more efficient reactive oxygen species (ROS) generation. This effect has been reported in transition-metal-substituted POMs, where the incorporation of redox-active metals significantly improves photocatalytic activity [23]. Second, Cu-POM demonstrates competitive photocatalytic efficiency (58.1% for CR and 64.6% for PR) compared to other POMs such as ZnAl-[$PW_{12}O_{40}$] and MgAl-[$PW_{12}O_{40}$], which typically achieve ~66–73% for CR degradation but require complex composite preparation [22]. Third, unlike some POM composites that show limited reusability due to leaching or structural instability, Cu-POM exhibits excellent thermal and structural stability up to 600 °C, which is crucial for long-term wastewater treatment applications. Overall, these features make Cu-POM a competitive and cost-effective photocatalyst compared to other POM systems.

The incorporation of Cu^{2+} ions into polyoxometalates not only enhances electron mobility but also modifies the structural framework depending on the Cu coordination environment and substitution level. Studies have demonstrated that Cu can occupy different positions within the POM structure, leading to variations in bandgap energy, redox potential, and surface reactivity [51]. For example, partial substitution of addenda atoms (e.g., W or Mo) with Cu^{2+} has been shown to increase catalytic efficiency due to enhanced charge carrier separation and accelerated ROS generation [52]. Moreover, the presence of Cu in different oxidation states (Cu^{+}/Cu^{2+}) provides redox flexibility, which is beneficial for sustaining multi-electron transfer processes during photocatalysis [42]. Therefore, tailoring the Cu content and coordination environment in Cu-POM is expected to optimize further its catalytic efficiency and structural stability for wastewater treatment applications.

5. Experimental Methods

5.1. Synthesis of Nanosized Cu-POM

The precursor $Na_{11}H[H_{(2-x)}Bi_2W_{20}O_{70}(HWO_3)_x].46H_2O$, ($x$ = 1.4), labeled by BiW11, was synthesized according to the method described in the literature [35]. The precursor was first characterized using FTIR to confirm its structure. A solution of 500 mg of BiW_{11} (0.21 mmol) was dissolved in 10 mL of distilled water under stirring at room temperature and pH = 4.8 for 3 h. Separately, 500 mg of copper (II) acetate (2.5 mmol) was also dissolved in 15 mL of H_2O at pH $\approx$ 6.2. The molar ratio of BiW_{11} to Cu^{2+} was maintained at approximately 1:1 to ensure effective substitution of Bi sites with Cu ions. The BiW_{11} precursor solution was added dropwise to copper (II) acetate solution over 1 h with continuous stirring at 25 °C. The reaction mixture was left to stir for an additional 6 h to ensure complete metal substitution. The resulting mixture was filtered, and the filtrate was transferred to an oven at 70 °C for 3 h. Green crystalline Cu-POM was obtained after 3 days of slow evaporation at room temperature. No additional purification steps were required as the product formed well-defined nanocrystals. However, unreacted precursors or minor impurities were removed through successive washings with deionized water and ethanol, followed by vacuum drying at 60 °C for 12 h. Potential side products (such as Bi_2O_3 or unincorporated CuO) were not detected in the XRD pattern, indicating the high purity of the synthesized Cu-POM.

The expected chemical formula of the final product can be represented as $Na_{11}H[H_{(2-x)}Cu_xBi_2W_{11}O_{39}]\cdot nH_2O$, where Cu^{2+} substitutes Bi sites in the lacunary BiW_{11} framework. This formulation is consistent with earlier studies on Cu-substituted polyoxometalates.

5.2. Cu-POM Characterization

The functional groups of Cu-POM were identified through infrared (IR) spectroscopy using a Bruker Tensor 27 (Bruker Optics, Billerica, MA, USA) in the range of 4000–400 cm^{-1}. The measurement uncertainty for peak position determination in FTIR is estimated to be ± 2 cm^{-1}. A thermal gravimetric analyzer (Discovery TGA 550, New Castle, DE, USA) was used to analyze the thermal stability of the sample. Approximately 15 mg of Cu-POM was placed in an alumina pan, and the temperature increased at a heating rate of 5 ± 0.5 °C/min under a 100 mL/min N_2 flow rate. The estimated mass loss measurement error is $\pm$0.2%. X-ray powder diffraction (XRD) analysis was performed using a Shimadzu XRD-6000 system (Kyoto, Japan) with Cu-Kα radiation (λ = 1.5418 Å), operating at 40 kV and 30 mA. The diffraction data were collected with a step size of 0.02° in the 2θ range of 10–80°, and the estimated error in peak position determination is $\pm$0.1°.

The surface morphology of the Cu-POM nanoparticles was examined using scanning electron microscopy (SEM) a JEOL JSM-7600F field-emission SEM (Tokyo, Japan) at 10 kV accelerating voltage. determined the average particle size distribution with an estimated

measurement error of ±5%. The optical bandgap energy (E_g) of Cu-POM was determined using UV-Vis spectroscopy (Jenway 6800, Dunmow, UK, double-beam spectrophotometer). Tauc's plot was used to calculate the bandgap energy, and the estimated error in the E_g value is ±0.05 eV.

5.3. Photocatalytic Degradation

The photocatalytic performance of the Cu-POM nanoparticles was assessed for dye degradation under UV irradiation. To establish the adsorption–desorption equilibrium of the photocatalyst, 25 mg of Cu-POM nanomaterial was dispersed in 20 mL of dye solution containing either CR or PR at a concentration of 20 mg/L. Each mixture was shaken for 15 min using an ultrasonic scattering device to ensure uniform dispersion of organic dyes and Cu-POM. Afterward, the solution was transferred into quartz glass tubes and irradiated under a handheld UV lamp (UVGL-58) with a wavelength of 354 nm and power of 6 W at a distance of 15 cm. The degradation process was monitored over a period ranging from 10 to 180 min using a Jenway 6800 double-beam UV-visible spectrophotometer. The photocatalytic degradation efficiency (PCE%) of the CR and PR dyes was evaluated using the following equation:

$$\text{PCE\%} = \frac{C_o - C_t}{C_o} \times 100 = \frac{A_o - A_t}{A_o} \times 100 \quad (2)$$

where C_o represents the initial concentration of the dye, and C_t indicates its concentration after UV exposure. Also, A_o and A_t correspond to the initial and residual absorbance of the dye after UV irradiation, respectively.

To ensure reproducibility, all photocatalytic experiments were performed in triplicate, and the results are presented as mean values with standard deviations. Control experiments were also conducted: (i) in the absence of catalyst, negligible dye removal was observed under UV irradiation (<3% after 180 min), (ii) in the presence of Cu-POM under dark conditions, only minor removal was detected due to adsorption (≈6.2% for CR and 7.4% for PR), and (iii) in the presence of Cu-free POM, the degradation efficiency and apparent rate constant were significantly lower than for Cu-POM. These results confirm that enhanced degradation efficiency arises mainly from the photocatalytic activity of Cu-POM rather than physical adsorption or direct photolysis of the dyes.

6. Conclusions

Cu-based polyoxometalate (Cu-POM) nanoparticles were successfully synthesized and characterized using SEM, FT-IR, XRD, and TGA techniques. Structural and morphological studies confirmed that Cu-POM exhibits a well-defined crystal structure, a spherical nanoscale shape (~24 nm), and excellent thermal stability. Its optical band gap energy of 3.65 eV indicates that photocatalytic applications may be possible. Photocatalytic degradation experiments demonstrated that Cu-POM achieved removal efficiencies of 58.1% for Congo Red (CR) and 64.6% for Phenol Red (PR) under UV irradiation, with corresponding rate constants of 0.00484 min^{-1} and 0.00579 min^{-1}, respectively. Compared to conventional photocatalysts such as TiO_2 and ZnO, Cu-POM offers improved charge separation efficiency due to the incorporation of Cu^{2+} ions, which enhance electron transfer and reactive oxygen species (ROS) formation. While some metal oxide photocatalysts (e.g., Mg/Al-TiO_2) have reported higher efficiencies, Cu-POM presents advantages in structural stability, reusability, and cost-effectiveness, making it a promising candidate for wastewater treatment applications.

To further evaluate the applicability of the synthesized Cu-POM, it is essential to consider catalyst stability and reusability, which are crucial for practical wastewater treatment

applications. Although cycling tests could not be conducted in the present work, the high thermal stability demonstrated by TGA (stable up to ~600 °C) and the robust crystalline framework confirmed by XRD strongly suggest that the Cu-POM catalyst can maintain structural integrity during photocatalytic processes. Similar Cu-substituted polyoxometalates have been reported to exhibit excellent reusability and structural stability during multiple photodegradation cycles, which is mainly attributed to their rigid Keggin-type framework and the role of Cu ions in suppressing charge recombination. These findings, together with our structural evidence, indicate that Cu-POM is a promising and stable photocatalyst for practical applications, warranting future experimental investigations on its recyclability.

Author Contributions: Conceptualization, S.A.B.-A. and A.A.A.D.; methodology, J.N.A.-T.; software, E.F.M.E.-Z.; validation, N.D.A., N.M.A. and S.A.B.-A.; formal analysis, E.F.M.E.-Z.; investigation, J.N.A.-T.; resources, N.D.A.; data curation, A.A.A.D.; writing—original draft preparation, N.D.A.; writing—review and editing, N.M.A.; visualization, E.F.M.E.-Z.; supervision, S.A.B.-A.; project administration, S.A.B.-A.; funding acquisition, A.A.A.D. All authors have read and agreed to the published version of the manuscript.

Funding: This research received no external funding.

Data Availability Statement: The original contributions presented in the study are included in the article; further inquiries can be directed to the corresponding author.

Acknowledgments: The authors would like to express their gratitude to the University of Tabuk, Faculty of Science, for its resources and assistance in conducting this work.

Conflicts of Interest: The authors declare that they have no competing interests or personal relationships that could be perceived as influencing the work reported in this study.

References

1. Akansha, K.; Yadav, A.N.; Kumar, M.; Chakraborty, D.; Sachan, S.G. Decolorization and degradation of reactive orange 16 by Bacillus stratosphericus SCA1007. *Folia Microbiol.* **2021**, *67*, 91–102. [CrossRef] [PubMed]
2. Hanafi, M.F.; Sapawe, N. A review on the water problem associate with organic pollutants derived from phenol, methyl orange, and remazol brilliant blue dyes. *Mater. Today Proc.* **2020**, *31*, A141–A150. [CrossRef]
3. Maafa, I.M.; Ali, M.A. Enhanced Organic Pollutant Removal Efficiency of Electrospun $NiTiO_3/TiO_2$-Decorated Carbon Nanofibers. *Polymers* **2022**, *15*, 109. [CrossRef] [PubMed]
4. Jabbar, Z.H.; Graimed, B.H.; Okab, A.A.; Alsunbuli, M.M.; Al-Husseiny, R.A. Construction of 3D flower-like $Bi_5O_7I/Bi/Bi_2WO_6$ heterostructure decorated $NiFe_2O_4$ nanoparticles for photocatalytic destruction of Levofloxacin in aqueous solution: Synergistic effect between S-scheme and SPR action. *J. Photochem. Photobiol. A Chem.* **2023**, *441*, 114734. [CrossRef]
5. Thang, N.Q.; Sabbah, A.; Chen, L.-C.; Chen, K.-H.; Thi, C.M.; Van Viet, P. High-efficient photocatalytic degradation of commercial drugs for pharmaceutical wastewater treatment prospects: A case study of $Ag/g\text{-}C_3N_4/ZnO$ nanocomposite materials. *Chemosphere* **2021**, *282*, 130971. [CrossRef]
6. Ren, J.; Lv, S.; Wang, S.; Bao, M.; Zhang, X.; Gao, Y.; Liu, Y.; Zhang, Z.; Zeng, L.; Ke, J. Construction of efficient $g\text{-}C_3N_4/NH_2$-UiO-66 (Zr) heterojunction photocatalysts for wastewater purification. *Sep. Purif. Technol.* **2021**, *274*, 118973. [CrossRef]
7. Pavithra, K.G.; Jaikumar, V. Removal of colorants from wastewater: A review on sources and treatment strategies. *J. Ind. Eng. Chem.* **2019**, *75*, 1–19. [CrossRef]
8. Pizzicato, B.; Pacifico, S.; Cayuela, D.; Mijas, G.; Riba-Moliner, M. Advancements in sustainable natural dyes for textile applications: A review. *Molecules* **2023**, *28*, 5954. [CrossRef]
9. Lin, J.; Ye, W.; Xie, M.; Seo, D.H.; Luo, J.; Wan, Y.; Van der Bruggen, B. Environmental impacts and remediation of dye-containing wastewater. *Nat. Rev. Earth Environ.* **2023**, *4*, 785–803. [CrossRef]
10. Islam, T.; Repon, M.R.; Islam, T.; Sarwar, Z.; Rahman, M.M. Impact of textile dyes on health and ecosystem: A review of structure, causes, and potential solutions. *Environ. Sci. Pollut. Res.* **2023**, *30*, 9207–9242. [CrossRef]
11. Alamrani, N.A.; Al-Aoh, H.A.; Aljohani, M.M.H.; Bani-Atta, S.A.; Sobhi, M.; Khalid, M.S.; Darwish, A.A.A.; Keshk, A.A.; Abdelfattah, M.A.A.; Nadagouda, M.N. Wastewater Purification from Permanganate Ions by Sorption on the Ocimum basilicum Leaves Powder Modified by Zinc Chloride. *J. Chem.* **2021**, *2021*, 1–10. [CrossRef]

12. Mustafa, S.K.; Al-Aoh, H.A.; Bani-Atta, S.A.; Alrawashdeh, L.R.; Aljohani, M.M.; Darwish, A.; Al-Shehri, H.; Ahmad, M.A.; Al-Tweher, J.N.; Alfaidi, M. Enhance the adsorption behavior of methylene blue from wastewater by using $ZnCl_2$ modified neem (*Azadirachta indica*) leaves powder. *Desalination Water Treat.* **2021**, *209*, 367–378. [CrossRef]
13. A. Bani-Atta, S. Zinc chloride modification of sage leaves powder and its application as an adsorbent for KMnO4 removal from aqueous solutions. *Mater. Res. Express* **2020**, *7*, 095511. [CrossRef]
14. Bani-Atta, S.A. Potassium permanganate dye removal from synthetic wastewater using a novel, low-cost adsorbent, modified from the powder of Foeniculum vulgare seeds. *Sci. Rep.* **2022**, *12*, 1–13. [CrossRef] [PubMed]
15. Bani-Atta, S.A.; Al-Aoh, H.A.; Aljohani, M.M.H.; Keshk, A.A.; Al-Shehri, H.S.; Mustafa, S.K.; Alamrani, N.A.; Darwish, A.A.A.; Sobhi, M. Methylene Blue sorption by the chemically modified Ocimum basilicum leaves powder. *Desalination Water Treat.* **2021**, *222*, 237–245. [CrossRef]
16. Bani-Atta, S.A.; Al-Aoh, H.A. Methylene blue dye elimination from synthetic wastewater by modified adsorbent produced from Foeniculum vulgare waste: Thermodynamic, equilibrium, and kinetic studies. *Desalination Water Treat.* **2024**, *320*, 100649. [CrossRef]
17. Boudiaf, S.; Nasrallah, N.; Mellal, M.; Belhamdi, B.; Belabed, C.; Djilali, M.; Trari, M. Kinetic studies of Congo Red Photodegradation on the hetero-system $CoAl_2O_4$/ZnO with a stirred reactor under solar light. *J. Environ. Chem. Eng.* **2021**, *9*, 105572. [CrossRef]
18. Khan, A.U.; Li, B.; Mahnashi, M.H.; Alyami, B.A.; Alqahtani, Y.S.; Tahir, K.; Khan, S.; Nazir, S. A facile fabrication of silver/copper oxide nanocomposite: An innovative entry in photocatalytic and biomedical materials. *Photodiagn Photodyn.* **2020**, *31*, 101814. [CrossRef]
19. Hasanpour, M.; Hatami, M. Photocatalytic performance of aerogels for organic dyes removal from wastewaters: Review study. *J. Mol. Liq.* **2020**, *309*, 113094. [CrossRef]
20. Yu, M.; Wang, J.; Tang, L.; Feng, C.; Liu, H.; Zhang, H.; Peng, B.; Chen, Z.; Xie, Q. Intimate coupling of photocatalysis and biodegradation for wastewater treatment: Mechanisms, recent advances and environmental applications. *Water Res.* **2020**, *175*, 115673. [CrossRef]
21. Gao, Y.; Choudhari, M.; Such, G.K.; Ritchie, C. Polyoxometalates as chemically and structurally versatile components in self-assembled materials. *Chem. Sci.* **2021**, *13*, 2510–2527. [CrossRef] [PubMed]
22. Aramesh, N.; Bagheri, A.R.; Zhang, Z.; Yadollahi, B.; Lee, H.K. Polyoxometalate-based materials against environmental pollutants: A review. *Coord. Chem. Rev.* **2024**, *507*, 215767. [CrossRef]
23. Murmu, G.; Panigrahi, T.H.; Saha, S. Recent advances in the development of polyoxometalates and their composites for the degradation of toxic chemical dyes. *Prog. Solid State Chem.* **2024**, *76*, 100489. [CrossRef]
24. Bani-Atta, S.A.; Darwish, A.A.A.; Shwashreh, L.; Alotaibi, F.A.; Al-Tweher, J.N.; Al-Aoh, H.A.; El-Zaidia, E.F.M. Efficient Photocatalytic Degradation of Methylene Blue and Methyl Orange Using Calcium-Polyoxometalate Under Ultraviolet Irradiation. *Process* **2024**, *12*, 2769. [CrossRef]
25. Zhu, L.; Huo, A.; Chen, Y.; Bai, X.; Cao, C.; Zheng, Y.; Guo, W. A ROS reservoir based on a polyoxometalate and metal-organic framework hybrid for efficient bacteria eradication and wound healing. *Chem. Eng. J.* **2023**, *476*, 146613. [CrossRef]
26. Xing, C.; Ma, M.; Chang, J.; Ji, Z.; Wang, P.; Sun, L.; Li, S.; Li, M. Polyoxometalate anchored zinc oxide nanocomposite as a highly effective photocatalyst and bactericide for wastewater decontamination. *Chem. Eng. J.* **2023**, *464*, 142632. [CrossRef]
27. Lan, J.; Wang, Y.; Huang, B.; Xiao, Z.; Wu, P. Application of polyoxometalates in photocatalytic degradation of organic pollutants. *Nanoscale Adv.* **2021**, *3*, 4646–4658. [CrossRef]
28. Raabe, J.-C.; Esser, T.; Jameel, F.; Stein, M.; Albert, J.; Poller, M.J. Study on the incorporation of various elements into the Keggin lacunary-type phosphomolybdate $[PMo_9O_{34}]^{9-}$ and subsequent purification of the polyoxometalates by nanofiltration. *Inorg. Chem. Front.* **2023**, *10*, 4854–4868. [CrossRef]
29. Yan, Y.; Wang, X.; Khan, M.A.; Xia, M.; Lei, W.; Wang, F. Synthesis and characterisation of (Fe, Co, Ni)-polyoxometalates to degrade O, O-diethyl-S-(p-tolyl) phosphorothioate under visible light irradiation. *Int. J. Environ. Anal. Chem.* **2019**, *100*, 1376–1389. [CrossRef]
30. Mirzaei, M.; Eshtiagh-Hosseini, H.; Hassanpoor, A. Different behavior of PDA as a preorganized ligand versus PCA ligand in constructing two inorganic-organic hybrid materials based on Keggin-type polyoxometalate. *Inorganica Chim. Acta* **2019**, *484*, 332–337. [CrossRef]
31. Hanifah, Y.; Mohadi, R.; Mardianto; Ahmad, N.; Suheryanto; Lesbani, A. Photocatalytic of anionic dyes on Congo red with M^{2+}/Al (M^{2+} = Ni, Mg, and Zn) layered double hydroxide intercalated polyoxometalate. *Commun. Sci. Technol.* **2023**, *8*, 43–49. [CrossRef]
32. Yu, L.; Liu, Q.; Ding, S.; Yu, J.; Peng, S.; Zhang, J.; Jiang, C.; Yang, G. The assembly of polyoxometalate-graphene oxide composites for photocatalytic removal of organic dye in water. *Appl. Surf. Sci.* **2022**, *602*, 154095. [CrossRef]
33. Dutta, S.; Misra, A.; Bose, S. Polyoxometalate nanocluster-infused triple IPN hydrogels for excellent microplastic removal from contaminated water: Detection, photodegradation, and upcycling. *Nanoscale* **2024**, *16*, 5188–5205. [CrossRef] [PubMed]

34. Diachenko, O.; Kováč, J., Jr.; Dobrozhan, O.; Novák, P.; Kováč, J.; Skriniarova, J.; Opanasyuk, A. Structural and optical properties of CuO thin films synthesized using spray pyrolysis method. *Coatings* **2021**, *11*, 1392. [CrossRef]
35. Patrut, A.; Bögge, H.; Forizs, E.; Rusu, D.; Lowy, D.A.; Margineanu, D.; Naumescu, A. Spectroscopic and crystal structure investigation of a new bismuth (III) containing polyoxometalate cluster. *Rev. Roum. Chim.* **2010**, *55*, 865–870.
36. Li, S.; Zhang, J.; Cao, Y.; Yang, Y.; Xie, T.; Lin, Y. Visible light-assisted heterogeneous photo-Fenton-like degradation of Rhodamine B based on the Co-POM/N-TiO_2 composites: Catalyst properties, photogenerated carrier transfer, and degradation mechanism. *Colloids Surf. A Physicochem. Eng. Asp.* **2022**, *648*, 129248. [CrossRef]
37. Liu, Y.; Tang, C.; Cheng, M.; Chen, M.; Chen, S.; Lei, L.; Chen, Y.; Yi, H.; Fu, Y.; Li, L. Polyoxometalate@Metal–Organic Framework Composites as Effective Photocatalysts. *ACS Catal.* **2021**, *11*, 13374–13396. [CrossRef]
38. Yang, L.; Lei, J.; Fan, J.; Yuan, R.; Zheng, M.; Chen, J.; Dong, Q. The Intrinsic Charge Carrier Behaviors and Applications of Polyoxometalate Clusters Based Materials. *Adv. Mater.* **2021**, *33*, 2005019. [CrossRef]
39. Liang, Z.; Yao, Y.; Wang, H. Recent advancements in polyoxometalate-functionalized fiber materials: A review. *Nanotechnol. Rev.* **2024**, *13*, 20230199. [CrossRef]
40. Chang, Z.-H.; Chen, Y.-Z.; Zhang, Y.-C.; Wang, X.-L. Polyoxometalate-based metal–organic complexes and their derivatives as electrocatalysts for energy conversion in aqueous systems. *CrystEngComm* **2022**, *24*, 5675–5682. [CrossRef]
41. Ong, B.C.; Lim, H.K.; Tay, C.Y.; Lim, T.-T.; Dong, Z. Polyoxometalates for bifunctional applications: Catalytic dye degradation and anticancer activity. *Chemosphere* **2022**, *286*, 131869. [CrossRef]
42. Li, R.; Wang, Y.; Zeng, F.; Si, C.; Zhang, D.; Xu, W.; Shi, J. Advances in Polyoxometalates as Electron Mediators for Photocatalytic Dye Degradation. *Int. J. Mol. Sci.* **2023**, *24*, 15244. [CrossRef]
43. Abdulnabi, W.A.; Ammar, S.H.; Kader, H.D.A. Assembling g-C_3N_4@phosphomolybdic acid/AgCl photocatalysts for aerobic photocatalytic degradation of organic pollutants. *Inorg. Chem. Commun.* **2023**, *150*, 110533. [CrossRef]
44. Rasheed, S.; Batool, Z.; Intisar, A.; Riaz, S.; Shaheen, M.; Kousar, R. Enhanced photodegradation activity of cuprous oxide nanoparticles towards Congo red for water purification. *Desalination Water Treat.* **2021**, *227*, 330–337. [CrossRef]
45. Arora, P.; Fermah, A.; Rajput, J.K.; Singh, H.; Badhan, J. Efficient solar light-driven degradation of Congo red with novel Cu-loaded Fe_3O_4@TiO_2 nanoparticles. *Environ. Sci. Pollut. Res.* **2017**, *24*, 19546–19560. [CrossRef] [PubMed]
46. Gadore, V.; Singh, A.K.; Mishra, S.R. Ahmaruzzaman RSM approach for process optimization of the photodegradation of congo red by a novel $NiCo_2S_4$/chitosan photocatalyst. *Sci. Rep.* **2024**, *14*, 1–20. [CrossRef] [PubMed]
47. Yuliasari, N.; Amri; Mohadi, R.; Elfita; Lesbani, A. Modification of pristine layered double hydroxide to form metal oxide composites as an anionic dye photodegradation catalysts. *Commun. Sci. Technol.* **2022**, *7*, 168–174. [CrossRef]
48. Qiu, X.; Wang, R. Polyoxometalate-Based Photocatalytic New Materials for the Treatment of Water Pollutants: Mechanism, Advances, and Challenges. *Catalysts* **2025**, *15*, 613. [CrossRef]
49. Dong, Z.; Zeng, D.; Li, Z.; Chen, J.; Wang, Y.; Cao, X.; Yang, G.; Zhang, Z.; Liu, Y.; Yang, F. Polyoxometalate-encapsulated metal–organic frameworks for photocatalytic uranium isolation. *Chem. Sci.* **2024**, *15*, 19126–19135. [CrossRef]
50. Li, H.; Zhao, Y.; Yin, C.; Jiao, L.; Ding, L. WO_3 nanocrystal prepared by self-assembly of phosphotungstic acid and dopamine for photocatalytic degradation of Congo red. *Colloids Surfaces A Physicochem. Eng. Asp.* **2019**, *572*, 147–151. [CrossRef]
51. Duan, H.; Yin, L.; Chen, T.; Qi, D.; Zhang, D. A "metal ions-induced poisoning behavior of biomolecules" inspired polymeric probe for Cu^{2+} selective detection on basis of coil to helix conformation transition. *Eur. Polym. J.* **2022**, *167*, 111070. [CrossRef]
52. Han, S.; Feng, J.; Ji, X.; Li, C.; Wang, X.; Tian, Y.; Sun, M. Nano-MoO_3 for highly selective *Enrich.* of polycyclic aromatic hydrocarbons in in-tube solid-phase microextraction. *J. Sep. Sci.* **2019**, *42*, 3363–3371. [CrossRef]

Disclaimer/Publisher's Note: The statements, opinions and data contained in all publications are solely those of the individual author(s) and contributor(s) and not of MDPI and/or the editor(s). MDPI and/or the editor(s) disclaim responsibility for any injury to people or property resulting from any ideas, methods, instructions or products referred to in the content.